Modeling State Transition and Head-Dependent Efficiency Curve for Pumped Storage Hydro in Look-Ahead Dispatch

Siyuan Wang, Jian Liu, Haotian Chen, Rui Bo, *Senior Member, IEEE*, Yonghong Chen, *Senior Member, IEEE*

***Abstract*—As one of the most widely installed utility-scale storage facilities, pumped storage hydro (PSH) plays an essential role in providing flexibility for power systems worldwide. Thus, to accurately quantify the flexibility of PSH units in operational optimization problems is important. The conventional PSH models in the literature rarely consider detailed state transitions due to their hourly-based settings. However, it becomes imperative for operational optimization on short-term intervals, especially with increasing shares of renewable energy in power systems. To this end, this paper presents a novel deterministic PSH model that considers the transition time and trajectory between three states of PSH units in look-ahead dispatch. Moreover, to better characterize the varying efficiency of PSH units with water head and flow rate, this paper proposes to model detailed head-dependent efficiency curves (hereafter called input-output curves) in look-ahead dispatch, which encounters heavy computational burdens when short time intervals are applied. In this work, a zig-zag piece-wise linear approximation method is used for input-output curve modeling. This can enable an accurate quantification for variable efficiency and head dependence in a computationally effective manner. Numerical results are presented to show performances of the proposed PSH model in both flexibility quantification and computation time.**

***Index Terms*—Pumped storage hydro, state transition, input-output curve, look-ahead dispatch.**

NOMENCLATURE

Indices and Sets

t	Index for time periods.
b, l	Index for buses and transmission lines.
g, h, w, d	Index for generators, PSH units, wind farms, and loads.
$\mathcal{T}$	Set of time periods in look-ahead horizon.
$\mathcal{G}, \mathcal{H}, \mathcal{W}, \mathcal{D}$	Set of generators, PSH units, wind farms, and loads.
$\mathcal{H}^r$	Set of PSH units connected to reservoir r.
$\mathcal{L}^b_{\text{from}}, \mathcal{L}^b_{\text{to}}$	Set of transmission lines from and to bus b.
$\cdot^b$	Set of equipment $\cdot$ at bus b.

Parameters

δt	Length of a time period [h].
$D_{d,t}$	Power consumption of load d during time period t [MW].
$W_{w,t}$	Power output from wind farm w during time period t [MW].
x_l	Reactance of transmission line l [p.u.].
F_l	Power rating of transmission line l [MW].
a_g, b_g, c_g	Coefficients of quadratic generation cost function for unit g [\$/h, \$/MWh, \$/MW^{2}h].
I	Number of pieces in generation cost piece-wise linear approximation.
β^i_g, γ^i_g	Coefficients of piece-wise linear generation cost for unit g in the i-th piece [\$/MW, \$].
$\hat{u}_{g,t}$	Unit commitment decision for unit g during time period t.
$\overline{P}_g$ ($\underline{P}_g$)	Maximum (minimum) power for unit g [MW].
RU_g(RD_g)	Upward (downward) ramp rate limit for unit g [MW/h].
c^{g}_h (c^{p}_h)	Generating (pumping) cost for PSH unit h [\$/MWh].
c^{ig}_h (c^{ip}_h, c^{pg}_h, c^{gp}_h)	Transition cost from idle to generating (idle to pumping, pumping to generating, and generating to pumping) for PSH unit h [\$].
$\overline{P}^{\text{g}}_h$ ($\overline{P}^{\text{p}}_h$)	Power rating for PSH unit h in generating (pumping) state [MW].
$\underline{P}^{\text{g}}_h$ ($\underline{P}^{\text{p}}_h$)	Minimum technical power for PSH unit h in generating (pumping) state [MW].
TT^{ig}_h (TT^{ip}_h, TT^{gi}_h, TT^{pi}_h, TT^{gp}_h, TT^{pg}_h)	Time periods required for state transitions of PSH unit h from idle to generating (idle to pumping, generating to idle, pumping to idle, generating to pumping, and pumping to generating).
$\hat{p}^{\text{ig}}_{h,t}$ ($\hat{p}^{\text{ip}}_{h,t}$, $\hat{p}^{\text{gi}}_{h,t}$, $\hat{p}^{\text{pi}}_{h,t}$, $\hat{p}^{\text{gp}}_{h,t}$, $\hat{p}^{\text{pg}}_{h,t}$)	Power trajectories for corresponding state transitions of PSH unit h [MW].
UT^{g}_h (UT^{p}_h)	Minimum on-line time periods for PSH unit h in generating (pumping) state.
DT_h	Minimum off-line time periods for PSH unit h.
Δ^{gp}_h (Δ^{pg}_h)	Indices of the last points before crossing zero in generating to pumping (pumping to generating) transition trajectory.
$\underline{V}_r$ ($\overline{V}_r$)	Lower (upper) volume bound for reservoir r [m^3]. Similarly, $\underline{V}_{r,\lvert\mathcal{T}\rvert}$ ($\overline{V}_{r,\lvert\mathcal{T}\rvert}$) represents

Manuscript received August 31, 2020; revised January 20, 2021 and April 29, 2021; accepted May 16, 2021. This material is based upon work supported by the U.S. Department of Energy's Office of Energy Efficiency and Renewable Energy (EERE) under the Water Power Technologies Office Award Number DE-EE0008781. The views expressed herein do not necessarily represent the views of the U.S. Department of Energy and the United States Government. Paper no. TPWRS-01486-2020. (*Corresponding author: Rui Bo.*)

Siyuan Wang, Jian Liu, Haotian Chen and Rui Bo are with the Department of Electrical and Computer Engineering, Missouri University of Science and Technology, MO 65409 USA (e-mail: siyuanwang@mst.edu; jliu@mst.edu; hc8xv@mst.edu; rbo@mst.edu).

Yonghong Chen is with Midcontinent Independent System Operator, Inc., Carmel, IN 46032 USA (e-mail: ychen@misoenergy.org).

This article has been accepted for publication in IEEE Transactions on Power Systems. DOI: 10.1109/TPWRS.2021.3084909.

lower (upper) volume bound for reservoir r at the end of look-ahead horizon [m^3].

$v_{r,0}$ Initial volume for reservoir r [m^3].

$m^{\mathrm{g}}, m^{\mathrm{p}}, n$ Numbers of discretization points on the generating flow rate, pumping power, and volume axis. The numbers of pieces are $m^{\mathrm{g}}-1, m^{\mathrm{p}}-1, n-1$, respectively.

$r^{\mathrm{g}}, r^{\mathrm{p}}, s$ Sizes of variables ς_k^{g}, $\varsigma_{k'}^{\mathrm{p}}$, and ζ_l.

$(\hat{q}_i^{\mathrm{g}}, \hat{v}_j, \hat{p}_{i,j}^{\mathrm{g}})$ Points obtained from $m^{\mathrm{g}} \times n$ discretization of the generating input-output curve.

$(\hat{p}_i^{\mathrm{p}}, \hat{v}_j, \hat{q}_{i,j}^{\mathrm{p}})$ Points obtained from $m^{\mathrm{p}} \times n$ discretization of the pumping input-output curve.

$\boldsymbol{C}^r$ Coefficient matrix for zig-zag formulations.

$C_{i,k}^r$ Entry in row i and column k of matrix $\boldsymbol{C}^r$.

Decision Variables

$\theta_{b,t}$ Voltage phase angle for bus b during time period t [rad].

$f_{l,t}$ Power flow for branch l during time period t [MW].

$p_{g,t}$ Power output from unit g during time period t [MW].

$wc_{w,t}$ Wind curtailment power for wind farm w during time period t [MW].

$\psi_{g,t}$ Cost for unit g during time period t [$].

$u_{h,t}^{\mathrm{g}}$ ($u_{h,t}^{\mathrm{p}}$, $u_{h,t}^{\mathrm{i}}$) Binary status variables that indicate PSH unit h is in generating (pumping, and idle, respectively) state during time period t, i.e., $u_{h,t}^{\mathrm{g}}=1$ when the unit is in generating state, and $u_{h,t}^{\mathrm{g}}=0$ otherwise.

$w_{h,t}^{\mathrm{ig}}$ ($w_{h,t}^{\mathrm{ip}}$, $w_{h,t}^{\mathrm{gi}}$, $w_{h,t}^{\mathrm{pi}}$, $w_{h,t}^{\mathrm{gp}}$, $w_{h,t}^{\mathrm{pg}}$) Binary variables that indicate state transition of PSH h from idle to generating (idle to pumping, generating to idle, pumping to idle, generating to pumping, and pumping to generating, respectively) during time period t, i.e., $w_{h,t}^{\mathrm{ig}}=1$ when the state is transited from idle to generating, and $w_{h,t}^{\mathrm{ig}}=0$ otherwise.

$p_{h,t}$ Network injection power from PSH unit h during time period t [MW].

$p_{h,t}^{\mathrm{g}}$ ($p_{h,t}^{\mathrm{p}}$) Generating (pumping) power from (to) PSH unit h during time period t [MW].

$q_{h,t}^{\mathrm{g}}$ ($q_{h,t}^{\mathrm{p}}$) Flow rates for PSH unit h during time period t in generating (pumping) state [m^3/s].

$v_{r,t}$ Volume of reservoir r during time period t [m^3].

$\phi_{i,j}^{\mathrm{g(p)}}$ Convex combination coefficient variable for zig-zag formulations (subscript h,t omitted).

$\varsigma_k^{\mathrm{g}}, \varsigma_{k'}^{\mathrm{p}}, \zeta_l$ Binary decision variables for binary zig-zag (ZZB) formulation (subscript h,t omitted).

$\tilde{\varsigma}_k^{\mathrm{g}}, \tilde{\varsigma}_{k'}^{\mathrm{p}}, \tilde{\zeta}_l$ Integer decision variables for integer zig-zag (ZZI) formulation (subscript h,t omitted).

$z_1^{\mathrm{g(p)}}, z_2^{\mathrm{g(p)}}$ Binary decision variables for triangular selections (subscript h,t omitted).

Ancillary Variables

$\tilde{u}_{h,t}^{\mathrm{g}}$ ($\tilde{u}_{h,t}^{\mathrm{p}}$, $\tilde{u}_{h,t}^{\mathrm{i}}$) Binary status variables that indicate PSH unit h is in generating (pumping, and idle, respectively) state but not in any transition process during time period t.

$\tilde{p}_{h,t}^{\mathrm{g}}$ ($\tilde{p}_{h,t}^{\mathrm{p}}$) Component of generating (pumping) power that excludes transition trajectory for PSH unit h during time period t [MW].

I. Introduction

PUMPED storage hydro (PSH) is one of the most widely installed utility-scale energy storage since its first use in the 1900s. According to DOE Global Energy Storage Database, the installed capacity of PSH reaches 181.1 GW in power systems worldwide as of January 2020, and it accounts for 94.8% of storage stations in terms of power rating [1]. With increasing shares of renewable energy in power systems, PSH can potentially offer its flexibility to address the intermittent power generation especially in short-term operations. Recently, look-ahead dispatch has drawn increasing attention by independent system operators [2], [3]. To exploit the flexibility of PSH, it is important to model PSH units in look-ahead dispatch with accurate flexibility quantification.

In the literature, PSH units are usually modeled as a mixed-integer representation using two [4]–[7] or three [8]–[10] binary variables for each unit and each time period. Recently, a configuration based PSH model was further proposed in [11] for day-ahead markets. Most previous optimizations are based on hourly time intervals, thus state transition behaviors are usually ignored in these PSH models. The state transition process of most PSH units can be implemented within an hour even for the most time-consuming generating to pumping transition. To better capture behaviors of intermittent power sources, shorter time intervals are required for operation models. As indicated in Table I, considering state transition time of PSH is of importance for real-time operation that typically runs at 5-minute intervals. It becomes particularly necessary for fixed speed PSH technology and for state transitions involving pumping. Moreover, the modeling of state transition trajectories can enable a more accurate flexibility quantification for PSH, especially when the fluctuations and the resulting power ramp rate of renewable energy sources are high.

Based on experiences of modeling traditional thermal units [14], [15] and combine cycle units [16] [17] in the literature, a novel PSH model that can quantify transition features of PSH units is proposed in this work. Importantly, we also investigated the value of our proposed model when short-term behaviors of intermittent energy sources are considered. In the case study, we will show how our proposed model differs from previous models in the flexibility performance of PSH units.

TABLE I
Typical Transition Time for Fixed Speed PSH

transition	reference [12]	reference [13]	
	normal FS[1]	advanced FS	extra fast response FS
idle to generating	$1-5$ min	1.5 min	1.3 min
idle to pumping	$3-30$ min	5.7 min	2.7 min
generating to pumping	$5-40$ min	7.0 min	4.0 min
pumping to generating	$2-20$ min	3.2 min	1.5 min

[1] FS represents fixed speed PSH.

In contrast to models that consider constant generating and pumping efficiencies, an input-output curve describes the relation between electric power, flow rate, and water head/volume, which can model various losses during the water-power conversion process. It is also referred to as hydropower production function in related literature. As the upper reservoir is usually a pond, most PSH units are head-dependent. In [5], a head-dependent PSH optimization model was proposed, which shows head effects on both of the generating and pumping states of the PSH units. Similar modeling methods have also been investigated in related hydropower literature. Piece-wise linear approximation methods can formulate the nonlinear input-output curve in a mixed-integer linear manner, which can be efficiently solved by on-the-shelf commercial solvers. In [18], a single variable piece-wise linear approximation method is performed by fixing multiple head levels, then electric power is estimated from a function that corresponds to a close head level. Authors of [19] and [20] further extended the three-piece case in [18] to general forms. A recent work in [21] summarized the piece-wise linear approximation approaches for conventional hydro production function modeling, and concluded the method proposed in [22] has the best performance.

Modeling the input-output curve could accurately quantify variable efficiency and head dependence for PSH units. However, when using shorter time intervals in optimizations, modeling the input-output curve encounters heavy computational burdens. In light of [23], we formulate the piece-wise linear input-output curve by using zig-zag approximation method, which can make the formulation stronger.

The contributions of this work are summarized as follows,

- We propose a novel deterministic PSH model for optimizations with sub-hourly time intervals. It considers detailed transition times and trajectories between pumping, generating, and idle states to capture the short-term behavior of PSH units. The proposed model can appropriately quantify the flexibility of PSH in wind power ramp events.
- We use a zig-zag piece-wise linear approximation method to model the input-output curve of PSH units, in order to address the computational burdens which would result from accurately modeling variable efficiency and head dependence features of water-power conversions.

II. Problem Formulation Considering Detailed State Transition

A. Look-Ahead Dispatch Framework

The mathematical model presented in this section is formulated for look-ahead dispatch, the framework of which has been extensively studied in the literature. Look-ahead dispatch can improve the efficiency and reliability of dispatch in renewable energy integrated power systems [24]. The look-ahead time frame of look-ahead dispatch is usually in a few hours. As a trade-off between performance and computation time, one hour is chosen in the case study of this work.

The interactions of look-ahead dispatch and day-ahead unit commitment (UC) can be achieved as follows: 1) Day-ahead UC decisions are applied to look-ahead dispatch for conventional generators. As PSH units are flexible to adjust, their operational decisions can be optimized in look-ahead dispatch. 2) For intertemporal water volume constraints of PSH units, in this paper we define bounds for volume at the end of look-ahead horizon. The bounds are determined according to day-ahead water volume solutions. An alternative option is to define a value-of-water function in the objective function [24], [25]. Our formulation can be easily adapted for this implementation.

B. Objective Function

As shown in (1), the objective function of look-ahead dispatch is the sum of generator cost (term a) and PSH cost (term b-1 and term b-2) in the optimization horizon. Generator cost $\psi_{g,t}$ is approximated by a piece-wise linear function in (5c). PSH cost consists of pumping/generating cost (term b-1) and state transition cost (term b-2).

$$\min \sum_{g\in\mathcal{G}}\sum_{t\in\mathcal{T}} \underbrace{\psi_{g,t}(p_{g,t})}_{\text{term a}} + \sum_{h\in\mathcal{H}}\sum_{t\in\mathcal{T}} \Big[\underbrace{(c_h^{\mathrm{g}}\cdot p_{h,t}^{\mathrm{g}} + c_h^{\mathrm{p}}\cdot p_{h,t}^{\mathrm{p}})\cdot\delta t}_{\text{term b-1}} + \underbrace{c_h^{\mathrm{ig}}\cdot w_{h,t}^{\mathrm{ig}} + c_h^{\mathrm{ip}}\cdot w_{h,t}^{\mathrm{ip}} + c_h^{\mathrm{pg}}\cdot w_{h,t}^{\mathrm{pg}} + c_h^{\mathrm{gp}}\cdot w_{h,t}^{\mathrm{gp}}}_{\text{term b-2}} \Big] \tag{1}$$

C. System Constraints

1) System Balance Constraints: The power balance constraints for all the buses and periods are expressed in (2).

$$\sum_{l\in\mathcal{L}_{\text{to}}^b} f_{l,t} - \sum_{l\in\mathcal{L}_{\text{from}}^b} f_{l,t} + \sum_{g\in\mathcal{G}^b} p_{g,t} + \sum_{h\in\mathcal{H}^b} p_{h,t} = \sum_{d\in\mathcal{D}^b} D_{d,t} - \sum_{w\in\mathcal{W}^b} (W_{w,t} - wc_{w,t}) \tag{2}$$

2) Transmission Line Constraints: The DC power flow and transmission line limit constraints are modeled in (3a) and (3b), respectively, wherein $l = (b_{\text{from}}, b_{\text{to}})$.

$$f_{l,t} = \left(\theta_{b_{\text{from}},t} - \theta_{b_{\text{to}},t}\right)/x_l \tag{3a}$$

$$-F_l \le f_{l,t} \le F_l \tag{3b}$$

D. Other Generator Constraints

1) Wind Curtailment Constraints: The upper and lower bounds for curtailed wind power are expressed in (4).

$$0 \le wc_{w,t} \le W_{w,t} \tag{4}$$

2) Conventional Generator Constraints: The upper and lower bounds, which are time-variant due to their dependence on day-ahead UC decisions $\hat{u}_{g,t}$, can be represented in (5a) for generators. Upward and downward ramp rate limits are expressed in (5b). As shown in (5c), we use piece-wise linear approximation to model the quadratic cost function $\psi_{g,t}(p_{g,t}) = (a_g\hat{u}_{g,t} + b_g p_{g,t} + c_g p_{g,t}^2)\cdot\delta t$.

$$\underline{P}_g\cdot\hat{u}_{g,t} \le p_{g,t} \le \overline{P}_g\cdot\hat{u}_{g,t} \tag{5a}$$

$$-RD_g\cdot\delta t\cdot\hat{u}_{g,t} \le p_{g,t} - p_{g,t-1} \le RU_g\cdot\delta t\cdot\hat{u}_{g,t} \tag{5b}$$

$$\beta_g^i\cdot p_{g,t} + \gamma_g^i\cdot\hat{u}_{g,t} \le \psi_{g,t} \quad \forall i\in[1,I]_{\mathbb{Z}} \tag{5c}$$

E. PSH Constraints

1) State Transition Logic: In order to ease our detailed state transition modeling, we formulate the transition logic based on the PSH model in [11]. Three binary variables $u^{\mathrm{g}}_{h,t}$, $u^{\mathrm{p}}_{h,t}$ and $u^{\mathrm{i}}_{h,t}$ are defined to represent the generating, pumping and idle states of PSH unit h, respectively. Six state transition variables are also introduced. A mutually exclusive relation is established in (6a), which ensures each PSH operates on one of the aforementioned states during each time period. Equation (6b) guarantees at most one state transition is allowed during each time period. The logic relations between state variables and transition variables are model in (6c)-(6e). As shown in Fig. 1a, transition variables $w^{\mathrm{ip}}_{h,t}$ and $w^{\mathrm{pi}}_{h,t}$ are on when state transition happens.

$$u^{\mathrm{g}}_{h,t} + u^{\mathrm{p}}_{h,t} + u^{\mathrm{i}}_{h,t} = 1 \tag{6a}$$

$$w^{\mathrm{ig}}_{h,t} + w^{\mathrm{ip}}_{h,t} + w^{\mathrm{gi}}_{h,t} + w^{\mathrm{pi}}_{h,t} + w^{\mathrm{gp}}_{h,t} + w^{\mathrm{pg}}_{h,t} \le 1 \tag{6b}$$

$$u^{\mathrm{g}}_{h,t} - u^{\mathrm{g}}_{h,t-1} = w^{\mathrm{ig}}_{h,t} + w^{\mathrm{pg}}_{h,t} - w^{\mathrm{gi}}_{h,t} - w^{\mathrm{gp}}_{h,t} \tag{6c}$$

$$u^{\mathrm{p}}_{h,t} - u^{\mathrm{p}}_{h,t-1} = w^{\mathrm{ip}}_{h,t} + w^{\mathrm{gp}}_{h,t} - w^{\mathrm{pi}}_{h,t} - w^{\mathrm{pg}}_{h,t} \tag{6d}$$

$$u^{\mathrm{i}}_{h,t} - u^{\mathrm{i}}_{h,t-1} = w^{\mathrm{gi}}_{h,t} + w^{\mathrm{pi}}_{h,t} - w^{\mathrm{ig}}_{h,t} - w^{\mathrm{ip}}_{h,t} \tag{6e}$$

2) State Transition Time: Considering the state transit process, we exclude the transition time periods from the status variables. For the generating mode, $\tilde{u}^{\mathrm{g}}_{h,t}$ is defined to indicate whether $p^{\mathrm{g}}_{h,t}$ reaches the minimum technical power $\underline{P}^{\mathrm{g}}_{h}$, and can be adjusted within $[\underline{P}^{\mathrm{g}}_{h}, \overline{P}^{\mathrm{g}}_{h}]$. For the pumping mode, $\tilde{u}^{\mathrm{g}}_{h,t}$ is used to indicate whether $p^{\mathrm{p}}_{h,t}$ reaches the minimum technical power $\underline{P}^{\mathrm{p}}_{h}$ for adjustable speed PSH, or the fixed pumping power $\overline{P}^{\mathrm{g}}_{h}$ for fixed speed PSH. For the idle mode, we trivially define $\tilde{u}^{\mathrm{i}}_{h,t} = u^{\mathrm{i}}_{h,t}$. As shown in Fig. 1a, $u^{\mathrm{g}}_{h,t} = 1$ holds for time periods 3-12, while $\tilde{u}^{\mathrm{g}}_{h,t} = 1$ applies only when $p^{\mathrm{p}}_{h,t}$ reaches $\overline{P}^{\mathrm{g}}_{h}$, i.e., time periods 6-10. When considering a pumping-to-generating transition, as shown in Fig. 1b, the transition time periods 12-13 are excluded for both $\tilde{u}^{\mathrm{p}}_{h,t}$ and $\tilde{u}^{\mathrm{g}}_{h,t}$. The detailed expression of $\tilde{u}^{\mathrm{g}}_{h,t}$, $\tilde{u}^{\mathrm{p}}_{h,t}$, and $\tilde{u}^{\mathrm{i}}_{h,t}$ are shown in (7a), (7b), and (7c), respectively.

$$\begin{aligned}\tilde{u}^{\mathrm{g}}_{h,t} \triangleq\ & u^{\mathrm{g}}_{h,t} - \sum_{\tau=1}^{\mathrm{TT}^{\mathrm{ig}}_{h}} w^{\mathrm{ig}}_{h,t-\tau+1} - \sum_{\tau=1}^{\mathrm{TT}^{\mathrm{gi}}_{h}} w^{\mathrm{gi}}_{h,t-\tau+\mathrm{TT}^{\mathrm{gi}}_{h}+1} \\ & - \sum_{\tau=1}^{\Delta^{\mathrm{gp}}_{h}} w^{\mathrm{gp}}_{h,t-\tau+\Delta^{\mathrm{gp}}_{h}+1} - \sum_{\tau=\Delta^{\mathrm{pg}}_{h}+1}^{\mathrm{TT}^{\mathrm{pg}}_{h}} w^{\mathrm{pg}}_{h,t-\tau+\Delta^{\mathrm{pg}}_{h}+1}\end{aligned} \tag{7a}$$

$$\begin{aligned}\tilde{u}^{\mathrm{p}}_{h,t} \triangleq\ & u^{\mathrm{p}}_{h,t} - \sum_{\tau=1}^{\mathrm{TT}^{\mathrm{ip}}_{h}} w^{\mathrm{ip}}_{h,t-\tau+1} - \sum_{\tau=1}^{\mathrm{TT}^{\mathrm{pi}}_{h}} w^{\mathrm{pi}}_{h,t-\tau+\mathrm{TT}^{\mathrm{pi}}_{h}+1} \\ & - \sum_{\tau=\Delta^{\mathrm{gp}}_{h}+1}^{\mathrm{TT}^{\mathrm{gp}}_{h}} w^{\mathrm{gp}}_{h,t-\tau+\Delta^{\mathrm{gp}}_{h}+1} - \sum_{\tau=1}^{\Delta^{\mathrm{pg}}_{h}} w^{\mathrm{pg}}_{h,t-\tau+\Delta^{\mathrm{pg}}_{h}+1}\end{aligned} \tag{7b}$$

$$\tilde{u}^{\mathrm{i}}_{h,t} \triangleq u^{\mathrm{i}}_{h,t} \tag{7c}$$

where Δ^{gp}_{h} and Δ^{pg}_{h} represent the indices of the last points before crossing zero in generating and pumping trajectories, respectively. The mathematical definitions are expressed in (8a) and (8b).

$$\Delta^{\mathrm{gp}}_{h} = \max_{\tau} \left\{ \tau : \tau \in [1, \mathrm{TT}_{h}]_{\mathbb{Z}},\ \hat{p}^{\mathrm{gp}}_{h,\tau} \ge 0 \right\} \tag{8a}$$

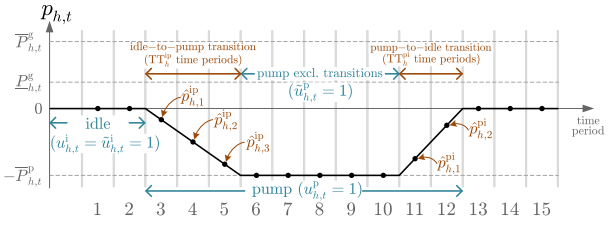

$u^{\mathrm{g}}_{h,t}$	0	0	0	0	0	0	0	0	0	0	0	0	0	0
$u^{\mathrm{p}}_{h,t}$	0	0	1	1	1	1	1	1	1	1	1	0	0	0
$u^{\mathrm{i}}_{h,t}$	1	1	0	0	0	0	0	0	0	0	0	1	1	1
$\tilde{u}^{\mathrm{g}}_{h,t}$	0	0	0	0	0	0	0	0	0	0	0	0	0	0
$\tilde{u}^{\mathrm{p}}_{h,t}$	0	0	0	0	0	1	1	1	1	1	0	0	0	0
$w^{\mathrm{ip}}_{h,t}$	0	0	1	0	0	0	0	0	0	0	0	0	0	0
$w^{\mathrm{pi}}_{h,t}$	0	0	0	0	0	0	0	0	0	0	0	1	0	0

(a)

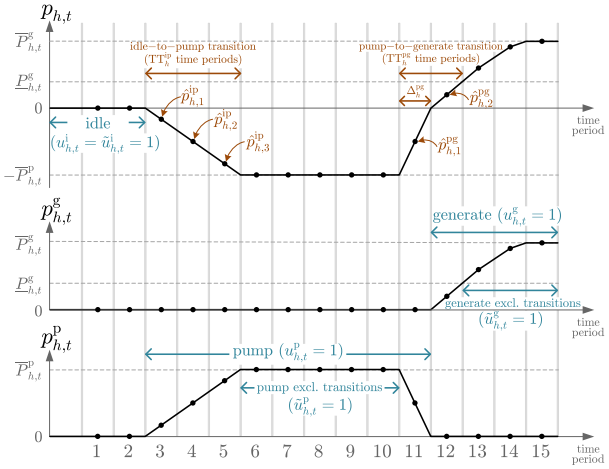

$u^{\mathrm{g}}_{h,t}$	0	0	0	0	0	0	0	0	0	0	1	1	1	1
$u^{\mathrm{p}}_{h,t}$	0	0	1	1	1	1	1	1	1	1	0	0	0	0
$u^{\mathrm{i}}_{h,t}$	1	1	0	0	0	0	0	0	0	0	0	0	0	0
$\tilde{u}^{\mathrm{g}}_{h,t}$	0	0	0	0	0	0	0	0	0	0	0	1	1	1
$\tilde{u}^{\mathrm{p}}_{h,t}$	0	0	0	0	0	1	1	1	1	1	0	0	0	0
$w^{\mathrm{ip}}_{h,t}$	0	0	1	0	0	0	0	0	0	0	0	0	0	0
$w^{\mathrm{pg}}_{h,t}$	0	0	0	0	0	0	0	0	0	0	1	0	0	0

(b)

Fig. 1. Illustrative examples for state transition logic, time periods and trajectories in a fixed speed PSH unit: (a) an example for idle-to-pumping and pumping-to-idle transitions; (b) an example that includes pumping-to-generating transition.

$$\Delta^{\mathrm{pg}}_{h} = \max_{\tau} \left\{ \tau : \tau \in [1, \mathrm{TT}^{\mathrm{pg}}_{h}]_{\mathbb{Z}},\ \hat{p}^{\mathrm{pg}}_{h,\tau} \le 0 \right\} \tag{8b}$$

With the definition of $\tilde{u}^{\mathrm{g}}_{h,t}$, the minimum on-line time constraint for the generating state can be expressed in (9a). This constraint follows the modeling idea in [14], and is further extended considering multiple transition variables and transition time. Analogously, (9b) and (9c) represent the minimum on-line time constraint for the pumping state and the minimum off-line time constraint, respectively.

$$\sum_{\tau=t-(\mathrm{TT}^{\mathrm{ig}}_{h}+\mathrm{UT}^{\mathrm{g}}_{h})+1}^{t-\mathrm{TT}^{\mathrm{ig}}_{h}} w^{\mathrm{ig}}_{h,\tau} + \sum_{\tau=t-(\mathrm{TT}^{\mathrm{pg}}_{h}-\Delta^{\mathrm{pg}}_{h}+\mathrm{UT}^{\mathrm{g}}_{h})+1}^{t-(\mathrm{TT}^{\mathrm{pg}}_{h}-\Delta^{\mathrm{pg}}_{h})} w^{\mathrm{pg}}_{h,\tau} \le \tilde{u}^{\mathrm{g}}_{h,t} \tag{9a}$$

$$\sum_{\tau=t-(\mathrm{TT}_h^{\mathrm{ip}}+\mathrm{UT}_h^{\mathrm{p}})+1}^{t-\mathrm{TT}_h^{\mathrm{ip}}} w_{h,\tau}^{\mathrm{ip}} + \sum_{\tau=t-(\mathrm{TT}_h^{\mathrm{gp}}-\Delta_h^{\mathrm{gp}}+\mathrm{UT}_h^{\mathrm{p}})+1}^{t-(\mathrm{TT}_h^{\mathrm{gp}}-\Delta_h^{\mathrm{gp}})} w_{h,\tau}^{\mathrm{gp}} \le \tilde{u}_{h,t}^{\mathrm{p}} \quad (9b)$$

$$\sum_{\tau=t-\mathrm{DT}_h+1}^{t} w_{h,\tau}^{\mathrm{gi}} + \sum_{\tau=t-\mathrm{DT}_h+1}^{t} w_{h,\tau}^{\mathrm{pi}} \le \tilde{u}_{h,t}^{\mathrm{i}} \quad (9c)$$

3) Power Constraints Considering State Transition Trajectory: The network injection power of PSH is defined as the difference of the generating power and pumping power in (10a). In (10b), we extend the modeling method in [15] to our generating power trajectory constraint considering state transitions of PSH. The generating power $p_{h,t}^{\mathrm{g}}$ is divided into two components: $\tilde{p}_{h,t}^{\mathrm{g}}$ is the component of generating power that excludes transition trajectory; other terms in the right hand side of (10b) composite the component of transition trajectory. The component that excludes transition trajectory is bounded in (10c). Analogously, the pumping power constraints are expressed in (10d)-(10e). The maximum ramp rates for both binary and ternary fixed speed PSH units are ranged from 1.7 to 2.1 MW/sec, while adjustable speed PSH units have even faster ramp rates to provide primary frequency response, which is referred to as 'flywheel effect' [26]. Thus, we do not model ramp rate constraints since PSH power can be adjusted without ramp rate limits in short time scales (eg, 5 min time interval for real-time operations).

$$p_{h,t} = p_{h,t}^{\mathrm{g}} - p_{h,t}^{\mathrm{p}} \quad (10a)$$

$$\begin{aligned} p_{h,t}^{\mathrm{g}} = \tilde{p}_{h,t}^{\mathrm{g}} &+ \sum_{\tau=1}^{\mathrm{TT}_h^{\mathrm{ig}}} \hat{p}_{h,\tau}^{\mathrm{ig}} \cdot w_{h,t-\tau+1}^{\mathrm{ig}} + \sum_{\tau=1}^{\mathrm{TT}_h^{\mathrm{gi}}} \hat{p}_{h,\tau}^{\mathrm{gi}} \cdot \\ & w_{h,t-\tau+\mathrm{TT}_h^{\mathrm{gi}}+1}^{\mathrm{gi}} + \sum_{\tau=\Delta_h^{\mathrm{pg}}+1}^{\mathrm{TT}_h^{\mathrm{pg}}} \hat{p}_{h,\tau}^{\mathrm{pg}} \cdot w_{h,t-\tau+\Delta_h^{\mathrm{pg}}+1}^{\mathrm{pg}} \\ &+ \sum_{\tau=1}^{\Delta_h^{\mathrm{gp}}} \hat{p}_{h,\tau}^{\mathrm{gp}} \cdot w_{h,t-\tau+\Delta_h^{\mathrm{gp}}+1}^{\mathrm{gp}} \end{aligned} \quad (10b)$$

$$\underline{P}_h^{\mathrm{g}} \cdot \tilde{u}_{h,t}^{\mathrm{g}} \le \tilde{p}_{h,t}^{\mathrm{g}} \le \overline{P}_h^{\mathrm{g}} \cdot \tilde{u}_{h,t}^{\mathrm{g}} \quad (10c)$$

$$\begin{aligned} p_{h,t}^{\mathrm{p}} = \tilde{p}_{h,t}^{\mathrm{p}} &+ \sum_{\tau=1}^{\mathrm{TT}_h^{\mathrm{ip}}} \left(-\hat{p}_{h,\tau}^{\mathrm{ip}}\right) \cdot w_{h,t-\tau+1}^{\mathrm{ip}} + \sum_{\tau=1}^{\mathrm{TT}_h^{\mathrm{pi}}} \left(-\hat{p}_{h,\tau}^{\mathrm{pi}}\right) \cdot \\ & w_{h,t-\tau+\mathrm{TT}_h^{\mathrm{pi}}+1}^{\mathrm{pi}} + \sum_{\tau=\Delta_h^{\mathrm{gp}}+1}^{\mathrm{TT}_h^{\mathrm{gp}}} \left(-\hat{p}_{h,\tau}^{\mathrm{gp}}\right) \cdot w_{h,t-\tau+\Delta_h^{\mathrm{gp}}+1}^{\mathrm{gp}} \\ &+ \sum_{\tau=1}^{\Delta_h^{\mathrm{pg}}} \left(-\hat{p}_{h,\tau}^{\mathrm{pg}}\right) \cdot w_{h,t-\tau+\Delta_h^{\mathrm{pg}}+1}^{\mathrm{pg}} \end{aligned} \quad (10d)$$

$$\underline{P}_h^{\mathrm{p}} \cdot \tilde{u}_{h,t}^{\mathrm{p}} \le \tilde{p}_{h,t}^{\mathrm{p}} \le \overline{P}_h^{\mathrm{p}} \cdot \tilde{u}_{h,t}^{\mathrm{p}} \quad (10e)$$

4) Water Volume Balance and Limits: To better capture the physical characteristics in engineering practice, energy constraints were modeled in reservoir volume form in [27]–[29]. Only the upper reservoir of PSH is modeled in most works, because the lower reservoir can be a lake, a river, or even an ocean, which contains a large volume of water. The water volume dynamics, bounds, and final level are modeled in (11). Natural inflow and evaporation are ignored in look-ahead dispatch time horizon.

$$v_{r,t} = v_{r,t-1} + \sum_{h\in\mathcal{H}^r} \left(q_{h,t}^{\mathrm{p}} - q_{h,t}^{\mathrm{g}}\right) \cdot 3600 \cdot \delta t \quad (11a)$$

$$\underline{V}_r \le v_{r,t} \le \overline{V}_r \quad (11b)$$

$$\underline{V}_{r,|\mathcal{T}|} \le v_{r,|\mathcal{T}|} \le \overline{V}_{r,|\mathcal{T}|} \quad (11c)$$

5) Input-Output Curve: The abstract form of the input-output curves for generating and pumping states are defined in (12a) and (12b), respectively. Note the flow rate $q_{h,t}^{\mathrm{p}}$ is represented as a function of the pumping power $p_{h,t}^{\mathrm{p}}$ for the pumping input-output curve. Detailed formulation for the input-output curves are given in the next section.

$$p_{h,t}^{\mathrm{g}} = \varphi_h^{\mathrm{g}}(q_{h,t}^{\mathrm{g}}, v_{h,t}) \quad (12a)$$

$$q_{h,t}^{\mathrm{p}} = \varphi_h^{\mathrm{p}}(p_{h,t}^{\mathrm{p}}, v_{h,t}) \quad (12b)$$

It should be pointed out that we cancel $\tilde{u}_{h,t}^{\mathrm{g}}$, $\tilde{u}_{h,t}^{\mathrm{p}}$, $\tilde{u}_{h,t}^{\mathrm{i}}$, $\tilde{p}_{h,t}^{\mathrm{g}}$, and $\tilde{p}_{h,t}^{\mathrm{p}}$ for a compact formulation when implementing the model. These ancillary variables are kept in the article for a clearer demonstration of the proposed model.

III. Input-Output Curve Approximation

Piece-wise linear approximation methods for input-output curve introduce extra integer variables to the model, which might increase the solution time significantly when the shorter time interval applies. To relieve the computational burden brought by modeling the input-output curve, a zig-zag approximation method is used in this work. The zig-zag formulation is compact and strong for piece-wise linear approximation [23]. In this section, we present two versions of the zig-zag based modeling approach that are proposed in [23], namely, integer zig-zag (ZZI) and binary zig-zag (ZZB). Performance comparisons of them in our PSH model are provided in the case study.

A. Binary Zig-zag based Modeling

The input-output curve for PSH is discretized and modeled through piece-wise linear approximation approaches. Taking the generating state an example, as shown in Fig. 2(a), a rectangular box is selected from the $m^{\mathrm{g}} \times n$ grid in the $(q_{h,t}^{\mathrm{g}}, v_{h,t})$ space. This is achieved by our proposed zig-zag formulations for PSH. As any four points in three-dimensional space are not necessary in the same plane, triangular selection

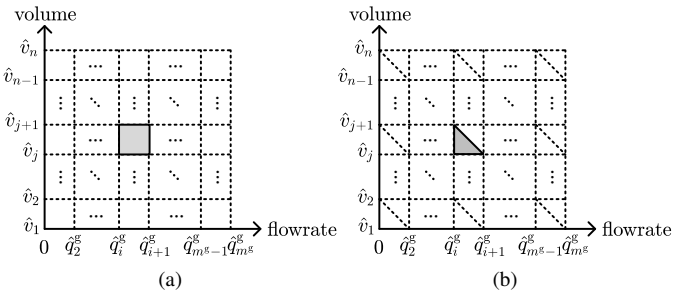

Fig. 2. Conceptual illustration of the zig-zag base input-output curve modeling: an example for the generating state. (a) rectangular selection (with zig-zag formulation); (b) triangular selection.

is then performed, as shown in Fig. 2(b). We omit the subscript h, t of all the variables for simplicity hereafter in this section.

1) ZZB Formulation: The ZZB approach uses binaries for decision variables in rectangular selection. The detailed formulation is shown in (13), in which (13a)-(13e) and (13f)-(13j) are designed for the generating and pumping states, respectively.

For the generating state, given discretized points $(\hat{q}_i^{\mathrm{g}}, \hat{v}_j, \hat{p}_{i,j}^{\mathrm{g}}),\ \forall i \in [1, m^{\mathrm{g}}]_{\mathbb{Z}},\ \forall j \in [1, n]_{\mathbb{Z}}$, decision variables $(q^{\mathrm{g}}, v, p^{\mathrm{g}})$ are represented as a convex combination of all the discretized points in (13a)-(13c) with continuous variables $\phi_{i,j}^{\mathrm{g}} \in [0, 1]$. A convex combination of three of these points is what we ultimately need to form a plane, which means the sum of only three $\phi_{i,j}^{\mathrm{g}}$ variables should equal to 1. Constraints (13d) and (13e) are used to limit the number of points in the convex combination to four (these four points correspond to four vertices of a rectangle as shown in Fig. 2(a)). Triangular selection, which is presented later in this section, further makes it to three. In fact, (13d) and (13e) are combinations of two special-ordered-sets-of-type-2 (SOS2) constraints. Each of them are modeled by using zig-zag formulations. In detail, constraint (13d) ensures at most two $\sum_{j=1}^{n} \phi_{i,j}^{\mathrm{g}}$ can be non-zero for all indices i. The same rule applies to $\sum_{i=1}^{m^{\mathrm{g}}} \phi_{i,j}^{\mathrm{g}}$ for all indices j in (13e). Finally, constraints (13b)-(13e) establish a convex combination representation of $(\hat{q}_i^{\mathrm{g}}, \hat{v}_j, \hat{p}_{i,j}^{\mathrm{g}})$, $(\hat{q}_{i+1}^{\mathrm{g}}, \hat{v}_j, \hat{p}_{i+1,j}^{\mathrm{g}})$, $(\hat{q}_i^{\mathrm{g}}, \hat{v}_{j+1}, \hat{p}_{i,j+1}^{\mathrm{g}})$, and $(\hat{q}_{i+1}^{\mathrm{g}}, \hat{v}_{j+1}, \hat{p}_{i+1,j+1}^{\mathrm{g}})$. The choices of i and j are decided according to the values of binary decision variables ς_k^{g} and ζ_l.

In a similar manner, constraints for the pumping state are constructed in (13f)-(13j), which can apply to both adjustable speed and fixed speed PSH units. Binary variables are declared in (13k). Note there exists no input-output curve that corresponds to the idle state, however, given $\hat{q}_i^{\mathrm{g}}$ and $\hat{p}_i^{\mathrm{p}}$ are zero for $i = 1$, an idle solution (i.e., $q^{\mathrm{g}}, q^{\mathrm{p}}, p^{\mathrm{g}}, p^{\mathrm{p}} = 0$ and $v \in [\underline{V}, \overline{V}]$) is valid in (13).

$$q^{\mathrm{g}} = \sum_{i=1}^{m^{\mathrm{g}}} \sum_{j=1}^{n} \hat{q}_i^{\mathrm{g}} \cdot \phi_{i,j}^{\mathrm{g}}, \quad v = \sum_{i=1}^{m^{\mathrm{g}}} \sum_{j=1}^{n} \hat{v}_j^{\mathrm{g}} \cdot \phi_{i,j}^{\mathrm{g}} \tag{13a}$$

$$p^{\mathrm{g}} = \sum_{i=1}^{m^{\mathrm{g}}} \sum_{j=1}^{n} \hat{p}_{i,j}^{\mathrm{g}} \cdot \phi_{i,j}^{\mathrm{g}} \tag{13b}$$

$$\sum_{i=1}^{m^{\mathrm{g}}} \sum_{j=1}^{n} \phi_{i,j}^{\mathrm{g}} = 1, \quad \phi_{i,j}^{\mathrm{g}} \geq 0 \tag{13c}$$

$$\sum_{i=1}^{m^{\mathrm{g}}} \left(C_{i-1,k}^{r^{\mathrm{g}}} \cdot \sum_{j=1}^{n} \phi_{i,j}^{\mathrm{g}} \right) \leq \varsigma_k^{\mathrm{g}} + \sum_{\ell=k+1}^{r^{\mathrm{g}}} 2^{\ell-k-1} \cdot \varsigma_\ell^{\mathrm{g}} \leq \sum_{i=1}^{m^{\mathrm{g}}} \left(C_{i,k}^{r^{\mathrm{g}}} \cdot \sum_{j=1}^{n} \phi_{i,j}^{\mathrm{g}} \right) \quad \forall k = [1, r^{\mathrm{g}}]_{\mathbb{Z}} \tag{13d}$$

$$\sum_{j=1}^{n} \left(C_{j-1,l}^{s} \cdot \sum_{i=1}^{m^{\mathrm{g}}} \phi_{i,j}^{\mathrm{g}} \right) \leq \zeta_l + \sum_{\ell=l+1}^{s} 2^{\ell-l-1} \cdot \zeta_\ell \leq \sum_{j=1}^{n} \left(C_{j,l}^{s} \cdot \sum_{i=1}^{m^{\mathrm{g}}} \phi_{i,j}^{\mathrm{g}} \right) \quad \forall l = [1, s]_{\mathbb{Z}} \tag{13e}$$

$$p^{\mathrm{p}} = \sum_{i=1}^{m^{\mathrm{p}}} \sum_{j=1}^{n} \hat{p}_i^{\mathrm{p}} \cdot \phi_{i,j}^{\mathrm{p}}, \quad v = \sum_{i=1}^{m^{\mathrm{p}}} \sum_{j=1}^{n} \hat{v}_j^{\mathrm{p}} \cdot \phi_{i,j}^{\mathrm{p}} \tag{13f}$$

$$q^{\mathrm{p}} = \sum_{i=1}^{m^{\mathrm{p}}} \sum_{j=1}^{n} \hat{q}_{i,j}^{\mathrm{p}} \cdot \phi_{i,j}^{\mathrm{p}} \tag{13g}$$

$$\sum_{i=1}^{m^{\mathrm{p}}} \sum_{j=1}^{n} \phi_{i,j}^{\mathrm{p}} = 1, \quad \phi_{i,j}^{\mathrm{p}} \geq 0 \tag{13h}$$

$$\sum_{i=1}^{m^{\mathrm{p}}} \left(C_{i-1,k'}^{r^{\mathrm{p}}} \cdot \sum_{j=1}^{n} \phi_{i,j}^{\mathrm{p}} \right) \leq \varsigma_{k'}^{\mathrm{p}} + \sum_{\ell=k'+1}^{r^{\mathrm{p}}} 2^{\ell-k'-1} \cdot \varsigma_\ell^{\mathrm{p}} \leq \sum_{i=1}^{m^{\mathrm{p}}} \left(C_{i,k'}^{r^{\mathrm{p}}} \cdot \sum_{j=1}^{n} \phi_{i,j}^{\mathrm{p}} \right) \quad k' = [1, r^{\mathrm{p}}]_{\mathbb{Z}} \tag{13i}$$

$$\sum_{j=1}^{n} \left(C_{j-1,l}^{s} \cdot \sum_{i=1}^{m^{\mathrm{p}}} \phi_{i,j}^{\mathrm{p}} \right) \leq \zeta_l + \sum_{\ell=l+1}^{s} 2^{\ell-l-1} \cdot \zeta_\ell \leq \sum_{j=1}^{n} \left(C_{j,l}^{s} \cdot \sum_{i=1}^{m^{\mathrm{p}}} \phi_{i,j}^{\mathrm{p}} \right) \quad \forall l = [1, s]_{\mathbb{Z}} \tag{13j}$$

$$\varsigma_k^{\mathrm{g}}, \varsigma_{k'}^{\mathrm{p}}, \zeta_l \in \{0, 1\}\ \forall k = [1, r^{\mathrm{g}}]_{\mathbb{Z}}, \forall k' = [1, r^{\mathrm{p}}]_{\mathbb{Z}}, \forall l = [1, s]_{\mathbb{Z}} \tag{13k}$$

where $r^{\mathrm{g}} = \lceil \log_2(m^{\mathrm{g}} - 1) \rceil$, $r^{\mathrm{p}} = \lceil \log_2(m^{\mathrm{p}} - 1) \rceil$, and $s = \lceil \log_2(n - 1) \rceil$ are sizes of binary variables ς_k^{g}, ζ_l, and $\varsigma_{k'}^{\mathrm{p}}$, respectively.

The coefficients in the ZZB formulation in (13d), (13e), (13i), and (13j) can be obtained in (14), wherein matrix $\boldsymbol{C}^r$ is defined in a recursive way (for simplicity, we use r to represent r^{g}, r^{p}, and s; use k to represent indices k, k', and l). Matrix size of $\boldsymbol{C}^r$ is $2^r \times r$. Denote $C_{i,k}^r$ as the entry in the i-th row and k-th column of matrix $\boldsymbol{C}^r$, and C_i^r as the i-th row vector of matrix $\boldsymbol{C}^r$. Specially, $C_{0,k}^r = C_{1,k}^r$ and $C_{2^r+1,k}^r = C_{2^r,k}^r$, $\forall k \in [1, r]_{\mathbb{Z}}$ are defined. This coefficient value selection is valid and efficient for SOS2 constraint modeling. Readers can refer to [23] for more details.

$$\boldsymbol{C}^1 = (0, 1)^\top \tag{14a}$$

$$\boldsymbol{C}^{r+1} = \begin{pmatrix} \boldsymbol{C}^r & \boldsymbol{0}^{2^r \times 1} \\ \boldsymbol{C}^r + \boldsymbol{1}^{2^r \times 1} \cdot C_{2^r}^r & \boldsymbol{1}^{2^r \times 1} \end{pmatrix}\ \forall r \in \mathbb{Z}^+ \tag{14b}$$

2) Triangular Selection: As mentioned previously, we use triangular selection to make sure at most three $\phi_{i,j}^{\mathrm{g}}$ values can be non-zero for the generating state in (13). Triangular selection constraints are provided in (15) to address this requirement using the method in [30]. The basic idea is to avoid simultaneous inclusion of four vertices of a rectangle in the (q^{g}, v) space. Four possible combinations of z_1^{g} and z_2^{g} values correspond to four anti-diagonal bands. Furthermore, the union of these bands covers all the triangles that we need. The detailed explanations in an illustrative example is provided in subsection III-C to better explain the triangular selection. The same constraints can be applied to the pumping state, as also shown in (15) without duplicating the constraints.

$$\sum_{(i,j) \in S_1} \phi_{i,j}^{\mathrm{g(p)}} \leq z_1^{\mathrm{g(p)}}, \quad \sum_{(i,j) \in S_2} \phi_{i,j}^{\mathrm{g(p)}} \leq 1 - z_1^{\mathrm{g(p)}} \tag{15a}$$

$$\sum_{(i,j) \in S_3} \phi_{i,j}^{\mathrm{g(p)}} \leq z_2^{\mathrm{g(p)}}, \quad \sum_{(i,j) \in S_4} \phi_{i,j}^{\mathrm{g(p)}} \leq 1 - z_2^{\mathrm{g(p)}} \tag{15b}$$

$$z_1^{\mathrm{g(p)}}, z_2^{\mathrm{g(p)}} \in \{0,1\} \tag{15c}$$

where the sets S_1 to S_4 are defined in (16). $a \equiv b \pmod c$ means a and b are congruent modulo c, i.e., $a - c \cdot \lfloor a/c \rfloor = b - c \cdot \lfloor a/c \rfloor$.

$$S_1 = \{(i,j) : i \equiv j \pmod 2 \text{ and } i+j \equiv 2 \pmod 4\} \tag{16a}$$
$$S_2 = \{(i,j) : i \equiv j \pmod 2 \text{ and } i+j \equiv 0 \pmod 4\} \tag{16b}$$
$$S_3 = \{(i,j) : i \not\equiv j \pmod 2 \text{ and } i+j \equiv 3 \pmod 4\} \tag{16c}$$
$$S_4 = \{(i,j) : i \not\equiv j \pmod 2 \text{ and } i+j \equiv 1 \pmod 4\} \tag{16d}$$

Finally, abstract input-output curve constraints (12) in section II can be implemented by ZZB-based formulations, as shown in (13) and (15).

B. Integer Zig-zag based Modeling

An alternative ZZI formulation, which uses integer rectangular selection variables, can be implemented by replacing (13d)-(13e), (13i)-(13j), and (13k) to (17a)-(17b), (17c)-(17d), and (17e), respectively. Constraints (17a)-(17b) are used for rectangular selection in the generating state, while corresponding constraints for the pumping state is shown in (17c)-(17d). Taking (13d) and (17a) as an example, the term $\varsigma_k^{\mathrm{g}} + \sum_{\ell=k+1}^{r^{\mathrm{g}}} 2^{\ell-k-1} \cdot \varsigma_\ell^{\mathrm{g}}$ in (13d) is naturally an integer, thus it can be equivalently replaced by an integer variable $\tilde{\varsigma}_k^{\mathrm{g}}$ in (17a). Integer variables are declared in (17e).

$$\sum_{i=1}^{m^{\mathrm{g}}} \left(C_{i-1,k}^{r^{\mathrm{g}}} \cdot \sum_{j=1}^{n} \phi_{i,j}^{\mathrm{g}} \right) \le \tilde{\varsigma}_k^{\mathrm{g}} \le \sum_{i=1}^{m^{\mathrm{g}}} \left(C_{i,k}^{r^{\mathrm{g}}} \cdot \sum_{j=1}^{n} \phi_{i,j}^{\mathrm{g}} \right) \quad \forall k = [1, r^{\mathrm{g}}]_{\mathbb{Z}} \tag{17a}$$

$$\sum_{j=1}^{n} \left(C_{j-1,l}^{s} \cdot \sum_{i=1}^{m^{\mathrm{g}}} \phi_{i,j}^{\mathrm{g}} \right) \le \tilde{\zeta}_l \le \sum_{j=1}^{n} \left(C_{j,l}^{s} \cdot \sum_{i=1}^{m^{\mathrm{g}}} \phi_{i,j}^{\mathrm{g}} \right) \quad \forall l = [1, s]_{\mathbb{Z}} \tag{17b}$$

$$\sum_{i=1}^{m^{\mathrm{p}}} \left(C_{i-1,k'}^{r^{\mathrm{p}}} \cdot \sum_{j=1}^{n} \phi_{i,j}^{\mathrm{p}} \right) \le \tilde{\varsigma}_{k'}^{\mathrm{p}} \le \sum_{i=1}^{m^{\mathrm{p}}} \left(C_{i,k'}^{r^{\mathrm{p}}} \cdot \sum_{j=1}^{n} \phi_{i,j}^{\mathrm{p}} \right) \quad \forall k' = [1, r^{\mathrm{p}}]_{\mathbb{Z}} \tag{17c}$$

$$\sum_{j=1}^{n} \left(C_{j-1,l}^{s} \cdot \sum_{i=1}^{m^{\mathrm{p}}} \phi_{i,j}^{\mathrm{p}} \right) \le \tilde{\zeta}_l \le \sum_{j=1}^{n} \left(C_{j,l}^{s} \cdot \sum_{i=1}^{m^{\mathrm{p}}} \phi_{i,j}^{\mathrm{p}} \right) \quad \forall l = [1, s]_{\mathbb{Z}} \tag{17d}$$

$$\tilde{\varsigma}_k^{\mathrm{g}}, \tilde{\varsigma}_{k'}^{\mathrm{p}}, \tilde{\zeta}_l \in \mathbb{Z} \quad \forall k = [1, r^{\mathrm{g}}]_{\mathbb{Z}},\ \forall k' = [1, r^{\mathrm{p}}]_{\mathbb{Z}}, \forall l = [1, s]_{\mathbb{Z}} \tag{17e}$$

C. An Illustrative Example

In this subsection, we show how the zig-zag approximation formulation works through an illustrative case in the 6-bus system in our case study. The ZZB formulation-based generating input-output curve approximation with 4 pieces ($m^{\mathrm{g}} = 5$ and $n = 5$) is taken as an example. The ZZI formulation can be understood in a similar manner. Let $\phi_i^{\mathrm{gq}} = \sum_{j=1}^{5} \phi_{i,j}^{\mathrm{g}}$ for the convenience of presentation. From (13c)-(13d), we have,

$$\phi_3^{\mathrm{gq}} + \phi_4^{\mathrm{gq}} + 2\phi_5^{\mathrm{gq}} \le \varsigma_1^{\mathrm{g}} + \varsigma_2^{\mathrm{g}} \le \phi_2^{\mathrm{gq}} + \phi_3^{\mathrm{gq}} + 2\phi_4^{\mathrm{gq}} + 2\phi_5^{\mathrm{gq}} \tag{18a}$$
$$\phi_4^{\mathrm{gq}} + \phi_5^{\mathrm{gq}} \le \varsigma_2^{\mathrm{g}} \le \phi_3^{\mathrm{gq}} + \phi_4^{\mathrm{gq}} + \phi_5^{\mathrm{gq}} \tag{18b}$$
$$\phi_1^{\mathrm{gq}} + \phi_2^{\mathrm{gq}} + \phi_3^{\mathrm{gq}} + \phi_4^{\mathrm{gq}} + \phi_5^{\mathrm{gq}} = 1 \tag{18c}$$
$$\phi_1^{\mathrm{gq}},\ \phi_2^{\mathrm{gq}},\ \phi_3^{\mathrm{gq}},\ \phi_4^{\mathrm{gq}},\ \phi_5^{\mathrm{gq}} \ge 0 \tag{18d}$$

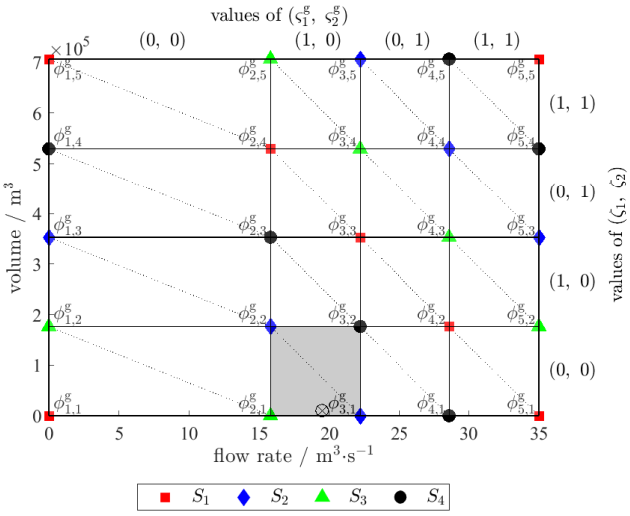

Fig. 3. An illustrative example for the zig-zag method

For example, if $\varsigma_1^{\mathrm{g}} = 0$ and $\varsigma_2^{\mathrm{g}} = 1$, $\phi_3^{\mathrm{gq}} + \phi_4^{\mathrm{gq}} + 2\phi_5^{\mathrm{gq}} \le 1 \le \phi_3^{\mathrm{gq}} + \phi_4^{\mathrm{gq}} + \phi_5^{\mathrm{gq}}$ can be obtained from the LHS of (18a) and the RHS of (18b), which indicates $\phi_5^{\mathrm{gq}} = 0$. Then we have $\phi_3^{\mathrm{gq}} + \phi_4^{\mathrm{gq}} \ge 1$. Considering (18c) and (18d), we further have $\phi_3^{\mathrm{gq}} + \phi_4^{\mathrm{gq}} = 1$, and $\phi_1^{\mathrm{gq}},\ \phi_2^{\mathrm{gq}},\ \phi_5^{\mathrm{gq}} = 0$. Under different combinations of ς_1^{g} and ς_2^{g}, the values of ϕ_i^{gq} are summarized in Table II. Analogously, by letting $\phi_j^{\mathrm{v}} = \sum_{i=1}^{5} \phi_{i,j}^{\mathrm{g}}$, the values of ϕ_j^{v} under different ζ_1 and ζ_2 follow the same rule in Table II.

Given the solution in time period 9 as an example, $(\varsigma_1^{\mathrm{g}}, \varsigma_2^{\mathrm{g}}, \zeta_1, \zeta_2) = (1,\ 0,\ 0,\ 0)$ implies $\phi_2^{\mathrm{gq}} + \phi_3^{\mathrm{gq}} = \sum_{j=1}^{5} \phi_{2,j}^{\mathrm{g}} + \sum_{j=1}^{5} \phi_{3,j}^{\mathrm{g}} = 1$ and $\phi_1^{\mathrm{v}} + \phi_2^{\mathrm{v}} = \sum_{i=1}^{5} \phi_{i,1}^{\mathrm{g}} + \sum_{i=1}^{5} \phi_{i,2}^{\mathrm{g}} = 1$. Considering (13c), as a result, $\phi_{2,1}^{\mathrm{g}} + \phi_{2,2}^{\mathrm{g}} + \phi_{3,1}^{\mathrm{g}} + \phi_{3,2}^{\mathrm{g}} = 1$. With the convex combination definition in (13a), the highlighted grid block in Fig. 3 corresponds to the $(1,\ 0,\ 0,\ 0)$ combination of $(\varsigma_1^{\mathrm{g}}, \varsigma_2^{\mathrm{g}}, \zeta_1, \zeta_2)$. Furthermore, each grid block in Fig. 3 corresponds to a combination of $(\varsigma_1^{\mathrm{g}}, \varsigma_2^{\mathrm{g}}, \zeta_1, \zeta_2)$ binary values.

Since any four points in the $(q^{\mathrm{g}}, v, p^{\mathrm{g}})$ space do not necessarily form a plane, triangular selection is necessary. The values $(z_1, z_2) = (0,\ 1)$ indicates $\phi_{i,j}^{\mathrm{g}} = 0$ for any $(i,j) \in S_1 \bigcup S_4$ from (15). As shown in Fig. 3, values of $\phi_{i,j}^{\mathrm{g}}$ for square markers (S_1) and circle markers (S_4) are zero. Thus, $\phi_{2,1}^{\mathrm{g}} + \phi_{2,2}^{\mathrm{g}} + \phi_{3,1}^{\mathrm{g}} = 1$, which forms the lower triangular region of the highlighted grid block. Then, as shown by the circular x-marker in Fig. 3, $(q^{\mathrm{g}}, v, p^{\mathrm{g}})$ is a convex combination of $(\hat{q}_2^{\mathrm{g}}, \hat{v}_1, \hat{p}_{2,1}^{\mathrm{g}})$, $(\hat{q}_2^{\mathrm{g}}, \hat{v}_2, \hat{p}_{2,2}^{\mathrm{g}})$, and $(\hat{q}_3^{\mathrm{g}}, \hat{v}_1, \hat{p}_{3,1}^{\mathrm{g}})$ for the PSH unit in time period 9. Given a grid block in Fig. 3, the choice in upper and lower triangles depends on the values of $(z_1^{\mathrm{g}}, z_2^{\mathrm{g}})$.

TABLE II
VALUES OF ϕ_i^{gq} UNDER DIFFERENT ς_1^{g} AND ς_2^{g}

ς_1^{g}	ς_2^{g}	ϕ_i^{gq}
0	0	$\phi_1^{\mathrm{gq}} + \phi_2^{\mathrm{gq}} = 1,\ \ \phi_3^{\mathrm{gq}} = \phi_4^{\mathrm{gq}} = \phi_5^{\mathrm{gq}} = 0$
1	0	$\phi_2^{\mathrm{gq}} + \phi_3^{\mathrm{gq}} = 1,\ \ \phi_1^{\mathrm{gq}} = \phi_4^{\mathrm{gq}} = \phi_5^{\mathrm{gq}} = 0$
0	1	$\phi_3^{\mathrm{gq}} + \phi_4^{\mathrm{gq}} = 1,\ \ \phi_1^{\mathrm{gq}} = \phi_2^{\mathrm{gq}} = \phi_5^{\mathrm{gq}} = 0$
1	1	$\phi_4^{\mathrm{gq}} + \phi_5^{\mathrm{gq}} = 1,\ \ \phi_1^{\mathrm{gq}} = \phi_2^{\mathrm{gq}} = \phi_3^{\mathrm{gq}} = 0$

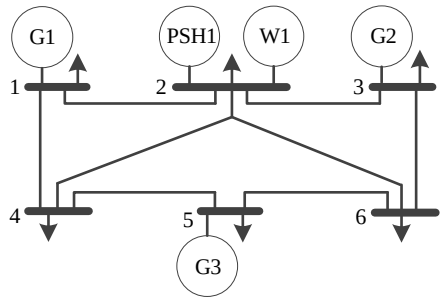

Fig. 4. Diagram for 6-bus system

IV. Case Study

In this section, we report our case studies on 6-bus, 118-bus, and 2383-bus systems. The 6-bus system is convenient for modeling enhancement demonstration, while 118-bus and 2383-bus systems are used for scalability tests. In this work, we use CPLEX 12.10 [31] to solve MILP problems on a computer with Intel Core i7-9700 CPU and 64 GB RAM.

A. 6-Bus System: Modeling Enhancement Analysis

1) System Settings: As shown in Fig. 4, the 6-bus system contains 3 thermal units, 1 wind farm, and 1 PSH unit, with 300 MW, 50 MW, and 30 MW installed capacities, respectively. Power bounds and minimum online/offline time period parameters for the PSH are listed in Table III. Table IV provides transition parameters for the PSH. The parameters for the reservoir are given in Table V.

In this case, the PSH input-output curve and reservoir modelings are expressed in (19). The input-output curve modelings (19a) and (19b) are from [20], [32]. Polynomial modeling of reservoir volume-head relation is shown in (19c).

$$p^{\mathrm{g}} = (\rho_0 + \rho_1 q^{\mathrm{g}} + \rho_2 q^{\mathrm{g}2} + \rho_3 \tilde{h} + \rho_4 \tilde{h}^2 + \rho_5 q^{\mathrm{g}} \tilde{h}) \cdot q^{\mathrm{g}} \tilde{h} \quad (19a)$$

$$\tilde{h} = \rho_6 + \rho_7 q^{\mathrm{p}} + \rho_8 q^{\mathrm{p}2} \quad (19b)$$

$$v = \rho_9 + \rho_{10} \tilde{h} + \rho_{11} \tilde{h}^2 \quad (19c)$$

where $\tilde{h}$ represents head of the reservoir. Subscripts are omitted for simplicity.

2) Accurate Flexibility Quantification through Sub-hourly Transition Modeling: In order to compare the PSH behaviors in our proposed model and previous models wherein detailed transitions are not considered, we experimented on a wind power ramp case. The time interval is set as 5 minutes to capture short-term wind power fluctuation. The optimization horizon is one hour during the evening peak load period, when the PSH unit is usually scheduled for generating in its daily cycle, and the reservoir volume is on a relatively low level. We set a target minimum terminal water level for the upper reservoir based on the day-ahead unit commitment decision.

When detailed state transition is modeled, the net-load/generation levels, PSH injection power, PSH status, and reservoir volume are shown in (b), (d), (f), and (h) subplots of Fig. 5, respectively. The corresponding results for the detailed-transition-ignored case are shown in (a), (c), (e), and (g) subplots of Fig. 5. If state transition times are ignored, we found the PSH unit can switch from generating state to pumping mode, and sequentially from pumping state to generating state very quickly. A series of of transitions from idle to pumping, and from pumping to idle are implemented in 10 minutes, as indicated in the highlighted part of Fig. 5 (c) and (e). This unrealistic modeling may overestimate the flexibility of most normal fixed speed PSH units. As shown in Fig. 5 (g) and (h), notice the detailed-transition-ignored solution generates more on the first 25 minutes, however when the pumped cannot be performed, the water in the upper reservoir may not be enough for the peak load in the remaining 35 minutes. A further cost analysis will be presented later.

Moreover, we find that the PSH unit frequently switches its status if detailed state transition is not modeled, which may be more suitable for the technical features of batteries. PSH units usually have longer-term cycles. When detailed state transition is considered, the PSH unit also generates to address the wind ramp event. However, as compared in Fig. 5 (e) and (f), the occurrence of state transitions is reduced.

Therefore, our proposed model can more realistically quantify the flexibility of PSH units. It accurately models the detailed state transitions and potentially reduces the short-term cycles, as PSH units are practically not feasible for such short-term cycles.

3) Cost Benefit from Sub-hourly Transition Modeling: We analyzed the flexibility quantification advantage of our proposed model from a solution feasibility perspective. It is also important to compare operational cost for both models in the real time. Now we show how solutions from the detailed-transition-ignored model can potentially increase system cost.

If PSH follows the dispatches from the detailed-transition-ignored model, when it runs to 25 minutes, operators would find PSH cannot transit to the pumping state so quickly. Then a corrective strategy is needed. In real-time operations, correc-

TABLE III
Unit Parameters for PSH in 6-Bus System

Bus	$\overline{P}^{\mathrm{g}}$	$\underline{P}^{\mathrm{g}}$	$\overline{P}^{\mathrm{p}}$
2	30.0 MW	7.3 MW	30.0 MW
$\underline{P}^{\mathrm{p}}$	UT^{g}	UT^{p}	DT
30.0 MW	2	2	2

TABLE IV
Unit Transition Parameters for PSH in 6-Bus System

transitions	time periods	trajectory
idle to generating	≈ 0	-
generating to idle	1	$[2.43]$
idle to pumping	3	$[-3.75, -7.50, -22.50]$
pumping to idle	2	$[-15.00, -7.50]$
generating to pumping	4	$[1.82, 0.91, -7.50, -22.50]$
pumping to generating	2	$[-15.00, 1.82]$

TABLE V
Reservoir Parameters for PSH in 6-Bus System

min head	max head	min volume	max volume
70.8 m	96.0 m	0 m^3	706064.5 m^3

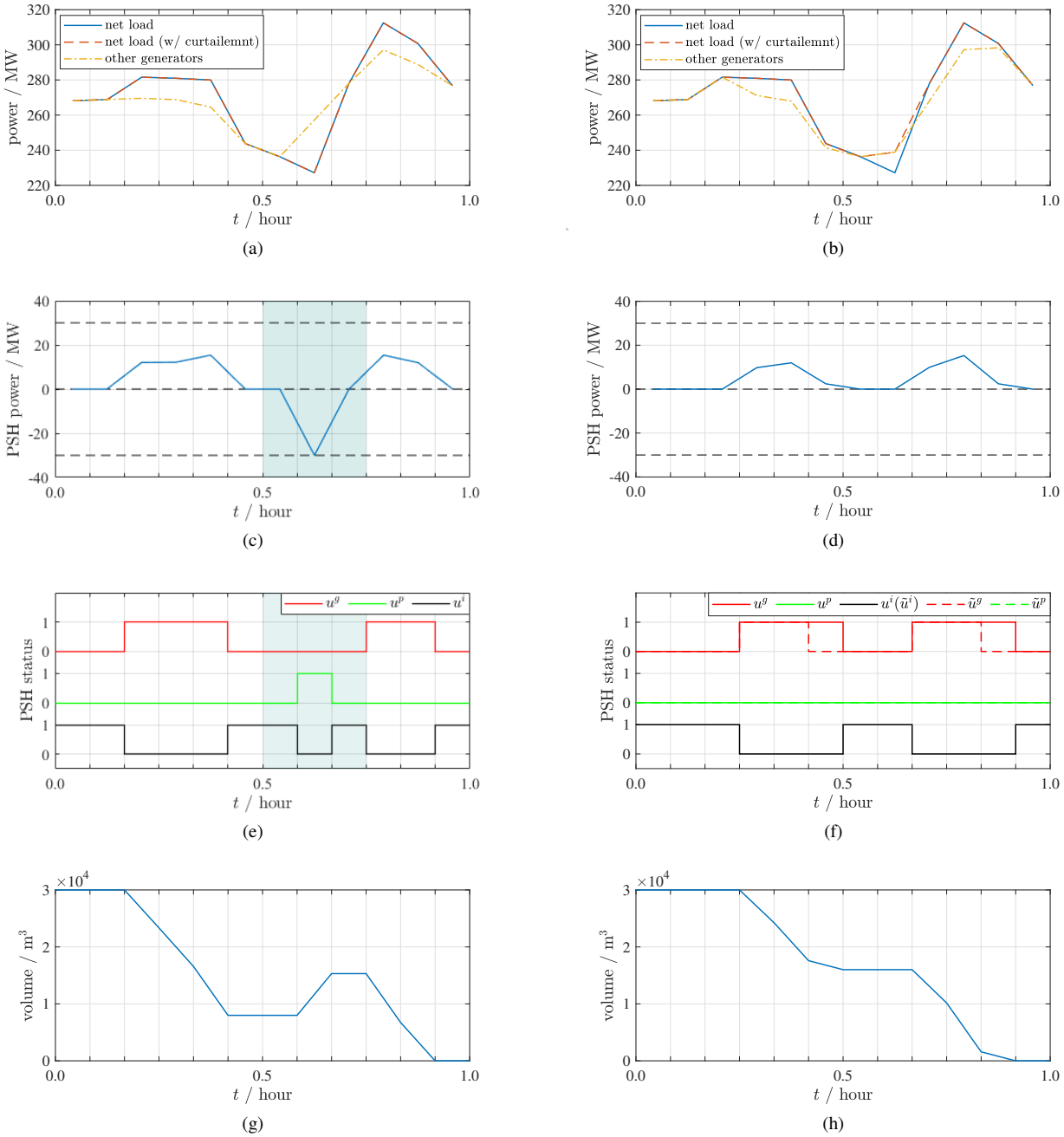

Fig. 5. Results comparison for 6 bus system: (a), (c), (e), (g) detailed transition ignored; (b), (d), (f), (h) detailed transition considered. Note the u^{p} and $\tilde{u}^{\mathrm{p}}$ curves (as well as some parts of the u^{g} and $\tilde{u}^{\mathrm{g}}$ curves) are overlapped in (f).

tive strategy could vary from different operation rules, which is difficult to model in general. As a conceptual illustration, we use our proposed model to re-optimizing a corrective strategy. A cost evaluation is conducted for the detailed-transition-ignored model in the following way:

- Follow the dispatch from the detailed-transition-ignored solution for first 25 minutes, which can be implemented through fixing respective dispatch in our proposed model.
- Re-optimize schedules for the remaining 35 minutes through making them free in the optimization model.

We notice the PSH generates more in the first 25 minutes by following the dispatch from the detailed-transition-ignored solution. This makes the PSH unable to supply in the peak load time periods in the remaining 35 minutes due to running out of water in the reservoir, thus load curtailment is mandatory.

TABLE VI
COST COMPARISONS

models	load shedding cost ($/MWh)	system cost ($)	shedded load (MWh)	curtailed wind (MWh)
detailed transition considered	-	2034.9	0	0.975
detailed transition ignored	50	2088.2	1.105	1.803
	100	2143.4	1.105	1.803

TABLE VII
MAXIMUM ERROR FOR DIFFERENT NUMBERS OF PIECES

number of pieces	max error percentage	number of pieces	max error percentage
2	11.1%	8	0.5%
4	2.2%	16	0.1%

To address the feasibility issue, load shedding variables and respective penalty cost terms are required to be included in the cost evaluation model. Given different load shedding cost settings, cost comparisons that we obtained are shown in Table VI. As indicated, accurate quantification of the flexibility of PSH units in a look-ahead dispatch can potentially reduce the cost in comparison to the formulation that ignores transition time modeling.

B. Scalability Test

We further use modified 118-bus [33] and 2383-bus [34] systems to test the scalability of the proposed model in larger systems. The computation time of zig-zag base piece-wise linear approximation formulation is important to test. In our numerical experiment, we use the formulation in [22] for comparison, which was named as logarithmic convex combination (LOG) and reported to be the most computationally efficient formulation currently in [21]. Taking a typical generating input-output curve as an example, as listed in Table VII, the maximum estimation error from piece-wise linear approximations is shown that input-output curve modeling is necessary, as 11.1% of capacity maximum error applies for the 2-piece case.

The 118-bus and 2383-bus systems are tested for the number of pieces from 2 to 16, with 0.1% and 0.5% gap settings, respectively. The look-ahead horizon is one hour in base cases, which is more practical for large systems. Considering the needs in near real time, time limits are set as 5 minutes. As the PSH units in the test systems are fixed-speed, for testing purpose, we change the number of pieces for generating flow rate and volume by assuming they are set as the same. The results for solution time of 118-bus and 2383-bus systems are shown in Table VIII and Table X, respectively. For each case, the fastest solution time among ZZI, ZZB, and LOG formulations is marked in bold. As indicated, the existing LOG formulation only wins a few cases, while the proposed ZZI formulation wins the most. Particularly, for time intensive cases, zig-zag approximation formulations perform better than the LOG formulation. Note in the 16-piece case of 2383-bus system, although ZZI doesn't reach the gap, it provides a high-quality solution.

Two sensitivity analyses are also performed in our numerical simulation. Table IX shows the testing results when the look-ahead horizon is extended to two hours in the 118-bus system. The performances of ZZI, ZZB, and LOG formulations align with the previous analysis. Congestion tests in the 2383-bus system are also conducted by reducing the transmission line limits on the base case. As indicated in Table XI, although computational performances are case dependent (i.e., more congested case may not necessarily take longer computation time), the ZZI formulation has better performance. Note in Table XI, as ZZB and LOG formulations do not converge in some cases, slightly different numbers of binding transmission line constraints appear for the same case setting.

Overall, compared with the existing LOG piece-wise linear approximation formulations in [21], [22] for the input-output curve modeling, the ZZI formulation can improve the computational time in most cases, and both ZZI and ZZB formulations perform better in time intensive cases.

TABLE VIII
COMPARISON FOR DIFFERENT NUMBER OF PIECES IN 118-BUS SYSTEM

number of pieces	ZZI		ZZB		LOG	
	time (s)	obj. (10^3\$)	time (s)	obj. (10^3\$)	time (s)	obj. (10^3\$)
2	**0.70**	59.6	**0.70**	59.6	0.83	59.6
4	3.33	59.6	2.64	59.6	**2.33**	59.6
6	4.95	59.6	**4.53**	59.6	5.13	59.6
8	**3.51**	59.6	4.67	59.6	5.39	59.6
10	6.47	59.6	6.66	59.6	**4.83**	59.6
12	**5.92**	59.6	9.09	59.6	8.45	59.6
14	8.97	59.6	**7.41**	59.6	7.48	59.6
16	**6.20**	59.6	9.63	59.6	10.42	59.6

TABLE IX
COMPARISON FOR DIFFERENT NUMBER OF PIECES IN 118-BUS SYSTEM (2 HOURS LOOK-AHEAD HORIZON)

number of pieces	ZZI		ZZB		LOG	
	time (s)	obj. (10^3\$)	time (s)	obj. (10^3\$)	time (s)	obj. (10^3\$)
2	**2.09**	100.2	2.64	100.2	3.30	100.2
4	18.45	100.2	9.50	100.2	**8.20**	100.2
6	**13.92**	100.3	31.77	100.2	16.81	100.2
8	28.06	100.2	47.63	100.2	**15.92**	100.2
10	**46.59**	100.2	51.09	100.2	50.63	100.2
12	**35.61**	100.2	73.91	100.2	112.70	100.2
14	**25.11**	100.2	67.95	100.2	76.53	100.2
16	**63.17**	100.2	96.09	100.2	137.91	100.3

TABLE X
COMPARISON FOR DIFFERENT NUMBER OF PIECES IN 2383-BUS SYSTEM

number of pieces	ZZI		ZZB		LOG	
	time (s)	obj. (10^3\$)	time (s)	obj. (10^3\$)	time (s)	obj. (10^3\$)
2	21.28	812.3	**16.44**	813.3	17.53	813.3
4	55.13	813.3	**48.33**	813.3	56.89	813.3
6	**102.22**	811.0	262.78	813.3	268.67	811.8
8	**52.25**	813.3	55.42	813.3	≥ 300	–
10	**214.63**	810.7	≥ 300	819.1	265.44	810.5
12	**171.26**	811.9	≥ 300	1413.6[1]	≥ 300	–
14	**202.08**	810.6	≥ 300	–	≥ 300	–
16	≥ 300	810.8	**293.97**	811.4	≥ 300	–

[1] As this case doesn't converge, only a feasible solution is found, which causes this irregularly large objective value.
[2] Symbol '–' indicates CPLEX doesn't find a feasible solution in 5 minutes.

TABLE XI
COMPARISON FOR DIFFERENT CONGESTION CONDITIONS IN 2383-BUS SYSTEM (8 PIECES)

case	ZZI		ZZB		LOG	
	time (s)	# of binding trans. cons.	time (s)	# of binding trans. cons.	time (s)	# of binding trans. cons.
base case	**52.25**	24	55.42	24	≥ 300	–
case 1	**279.59**	68	≥ 300	72	≥ 300	69
case 2	**160.05**	188	≥ 300	189	≥ 300	–

[1] Symbol '–' indicates CPLEX doesn't find a feasible solution in 5 minutes.

V. Conclusion

This paper presents a PSH model that considers sub-hourly state transitions and the detailed input-output curve for look-ahead dispatch. A zig-zag approximation-based formulation is used to model the input-output curves of PSH units. The generating part of this formulation can also be used for conventional hydro units. The conclusions of this work are,

- The proposed state transition model for PSH units can more realistically quantify the flexibility of PSH units, which might be overestimated in short-term operations if detailed state transition limits are ignored.
- Compared with using the current most computationally efficient piece-wise linear approximation method LOG [21], [22] in input-output curve modeling, the ZZI formulation can reduce the computational time in most cases, also both ZZI and ZZB formulations perform better in time intensive cases.

References

[1] Office of Electricity, DOE. DOE global energy storage database. [Online]. Available: https://www.energystorageexchange.org/

[2] Midcontinent ISO. Look ahead dispatch (IR064). [Online]. Available: https://www.misoenergy.org/stakeholder-engagement/issue-tracking/look-ahead-dispatch/

[3] California ISO. California independent system operator corporation fifth replacement FERC electric tariff. [Online]. Available: http://www.caiso.com/Documents/Conformed-Tariff-asof-Sep28-2019.pdf

[4] N. Li and K. W. Hedman, "Enhanced pumped hydro storage utilization using policy functions," *IEEE Transactions on Power Systems*, vol. 32, no. 2, pp. 1089–1102, 2016.

[5] C.-H. Chen, N. Chen, and P. B. Luh, "Head dependence of pump-storage-unit model applied to generation scheduling," *IEEE Transactions on Power Systems*, vol. 32, no. 4, pp. 2869–2877, 2016.

[6] M. Chazarra, J. I. Pérez-Díaz, and J. Garcia-Gonzalez, "Optimal joint energy and secondary regulation reserve hourly scheduling of variable speed pumped storage hydropower plants," *IEEE Transactions on Power Systems*, vol. 33, no. 1, pp. 103–115, 2017.

[7] J.-F. Toubeau, Z. De Grève, P. Goderniaux, F. Vallée, and K. Bruninx, "Chance-constrained scheduling of underground pumped hydro energy storage in presence of model uncertainties," *IEEE Transactions on Sustainable Energy*, vol. 11, no. 3, pp. 1516–1527, 2019.

[8] M. E. Khodayar, M. Shahidehpour, and L. Wu, "Enhancing the dispatchability of variable wind generation by coordination with pumped-storage hydro units in stochastic power systems," *IEEE Transactions on Power Systems*, vol. 28, no. 3, pp. 2808–2818, 2013.

[9] M. E. Khodayar, L. Abreu, and M. Shahidehpour, "Transmission-constrained intrahour coordination of wind and pumped-storage hydro units," *IET Generation, Transmission & Distribution*, vol. 7, no. 7, pp. 755–765, 2013.

[10] A. Golshani, W. Sun, Q. Zhou, Q. P. Zheng, J. Wang, and F. Qiu, "Coordination of wind farm and pumped-storage hydro for a self-healing power grid," *IEEE Transactions on Sustainable Energy*, vol. 9, no. 4, pp. 1910–1920, 2018.

[11] B. Huang, Y. Chen, and R. Baldick. A configuration based pumped storage hydro model in MISO day-ahead market [v1]. [Online]. Available: https://arxiv.org/abs/2009.04944

[12] P. Donalek, B. Trouille, P. Hartel, K. King, M. Bhattarai, R. Krohn, K. Gilbert, H. Lee, and J. Haapala, "Technical analysis of pumped storage and integration with wind power in the pacific northwest," MWH Americas, Inc., Tech. Rep., 2009.

[13] A. Botterud, T. Levin, and V. Koritarov, "Pumped storage hydropower: benefits for grid reliability and integration of variable renewable energy," Argonne National Lab., Tech. Rep., 2014.

[14] D. Rajan, S. Takriti *et al.*, "Minimum up/down polytopes of the unit commitment problem with start-up costs," *IBM Res. Rep*, vol. 23628, pp. 1–14, 2005.

[15] G. Morales-España, J. M. Latorre, and A. Ramos, "Tight and compact MILP formulation of start-up and shut-down ramping in unit commitment," *IEEE Transactions on Power Systems*, vol. 28, no. 2, pp. 1288–1296, 2012.

[16] L. Fan and Y. Guan, "An edge-based formulation for combined-cycle units," *IEEE Transactions on Power Systems*, vol. 31, no. 3, pp. 1809–1819, 2015.

[17] B. Hua, B. Huang, R. Baldick, and Y. Chen, "Tight formulation of transition ramping of combined cycle units," *IEEE Transactions on Power Systems*, vol. 35, no. 3, pp. 2167–2175, 2019.

[18] A. J. Conejo, J. M. Arroyo, J. Contreras, and F. A. Villamor, "Self-scheduling of a hydro producer in a pool-based electricity market," *IEEE Transactions on Power Systems*, vol. 17, no. 4, pp. 1265–1272, 2002.

[19] A. Borghetti, C. D'Ambrosio, A. Lodi, and S. Martello, "An MILP approach for short-term hydro scheduling and unit commitment with head-dependent reservoir," *IEEE Transactions on Power Systems*, vol. 23, no. 3, pp. 1115–1124, 2008.

[20] B. Tong, Q. Zhai, and X. Guan, "An MILP based formulation for short-term hydro generation scheduling with analysis of the linearization effects on solution feasibility," *IEEE Transactions on Power Systems*, vol. 28, no. 4, pp. 3588–3599, 2013.

[21] B. Brito, E. Finardi, and F. Takigawa, "Mixed-integer nonseparable piecewise linear models for the hydropower production function in the unit commitment problem," *Electric Power Systems Research*, vol. 182, p. 106234, 2020.

[22] J. P. Vielma and G. L. Nemhauser, "Modeling disjunctive constraints with a logarithmic number of binary variables and constraints," *Mathematical Programming*, vol. 128, no. 1-2, pp. 49–72, 2011.

[23] J. Huchette and J. P. Vielma, "Nonconvex piecewise linear functions: Advanced formulations and simple modeling tools," *Operations Research*, to appear.

[24] J. Zhao, T. Zheng, and E. Litvinov, "A multi-period market design for markets with intertemporal constraints," *IEEE Transactions on Power Systems*, vol. 35, no. 4, pp. 3015–3025, 2019.

[25] Y. Gu, J. Bakke, Z. Zhou, D. Osborn, T. Guo, and R. Bo, "A novel market simulation methodology on hydro storage," *IEEE Transactions on Smart Grid*, vol. 5, no. 2, pp. 1119–1128, 2014.

[26] V. Koritarov, T. D. Veselka, J. Gasper, B. M. Bethke, A. Botterud, J. Wang, M. Mahalik, Z. Zhou, C. Milostan, J. Feltes *et al.*, "Modeling and analysis of value of advanced pumped storage hydropower in the United States," Argonne National Lab.(ANL), Argonne, IL (United States), Tech. Rep., 2014.

[27] R. Allan, R. Li, and M. Elkateb, "Modelling of pumped-storage generation in sequential Monte Carlo production simulation," *IEE Proceedings-Generation, Transmission and Distribution*, vol. 145, no. 5, pp. 611–615, 1998.

[28] J. Garcia-Gonzalez, R. M. R. de la Muela, L. M. Santos, and A. M. Gonzalez, "Stochastic joint optimization of wind generation and pumped-storage units in an electricity market," *IEEE Transactions on Power Systems*, vol. 23, no. 2, pp. 460–468, 2008.

[29] P.-H. Chen, "Pumped-storage scheduling using evolutionary particle swarm optimization," *IEEE Transactions on Energy Conversion*, vol. 23, no. 1, pp. 294–301, 2008.

[30] J. Huchette and J. P. Vielma, "A combinatorial approach for small and strong formulations of disjunctive constraints," *Mathematics of Operations Research*, vol. 44, no. 3, pp. 793–820, 2019.

[31] IBM. ILOG CPLEX Homepage. Armonk, NY, USA. [Online]. Available: http://www.ilog.com

[32] M. Moreno, P. Planells, J. Córcoles, J. Tarjuelo, and P. Carrión, "Development of a new methodology to obtain the characteristic pump curves that minimize the total cost at pumping stations," *Biosystems Engineering*, vol. 102, no. 1, pp. 95–105, 2009.

[33] IIT. Data for IEEE 118-bus system. Chicago, IL, USA. [Online]. Available: http://motor.ece.iit.edu/data/SCUC_118/SCUC_118.xls

[34] R. D. Zimmerman and C. E. Murillo-Sanchez. MATPOWER (Version 7.1). Ithaca, NY, USA. [Online]. Available: https://matpower.org/

Siyuan Wang received the B.S. and Ph.D. degrees in electrical engineering from the College of Electrical Engineering, Zhejiang University, Hangzhou, China, in 2013 and 2019, respectively. He is currently a Postdoctoral Fellow with the Department of Electrical and Computer Engineering, Missouri University of Science and Technology (formerly University of Missouri-Rolla), Rolla, MO, USA. His research interests include power system planning and operation, renewable energy integration, and the application of energy storage technology in power systems.

Jian Liu received the B.S. and M.S. degrees in Mathematics and System Engineering from Linyi University and Xiamen University, in 2005 and 2009, respectively. He is pursuing the Ph.D. degree at the Missouri University of Science and Technology, Rolla, Missouri. His current interests include power system operation, energy storage, and energy market.

Haotian Chen received the B.S. degree in Physics from University of Science and Technology of China, Hefei, China, in 2013, and the M.S. degree in Computer Engineering from Florida Institute of Technology, Melbourne, Florida, in 2016. He is currently pursuing the Ph.D. degree at Missouri University of Science and Technology, Rolla, Missouri. His research interests include the power system economics and machine learning application in electricity market.

Rui Bo (Senior Member, IEEE) received the BSEE and MSEE degrees in electric power engineering from Southeast University (China) in 2000 and 2003, respectively, and received the Ph.D. degree from the University of Tennessee, Knoxville (UTK) in 2009. He is currently an Assistant Professor of the Electrical and Computer Engineering Department with the Missouri University of Science and Technology (formerly University of Missouri-Rolla). He worked as a Principal Engineer and Project Manager at Midcontinent Independent System Operator (MISO) from 2009 to 2017. His research interests include computation, optimization and economics in power system operation and planning, high performance computing, electricity market simulation, evaluation and design.

Yonghong Chen (Senior Member, IEEE) received the B.S. degree from Southeast University, Nanjing, China, the M.S. degree from Nanjing Automation Research Institute, China, and the Ph.D. degree from Washington State University, Pullman, WA, USA, all in electrical engineering. She also received the M.B.A. degree from Indiana University, Kelly School of Business, Indianapolis, IN, USA. She is currently a Consulting Advisor at MISO. In this role, she focuses on R&D to address challenges on market design and market clearing system. Before joining MISO in 2002, she worked with GridSouth Transco LLC and Nanjing Automation Research Institute.